The influence of synoptic weather regimes on UK air quality: regional model studies of tropospheric column NO$_2$

R. J. Pope[1,2]**, N. H. Savage**[3]**, M. P. Chipperfield**[1,2]**, C. Ordóñez**[3]**, and L. S. Neal**[3]

[1]School of Earth and Environment, University of Leeds, Leeds LS2 9JT, UK
[2]National Centre for Earth Observation, University of Leeds, Leeds LS2 9JT, UK
[3]Met Office, Exeter, UK

Correspondence to: R. J. Pope (earrjpo@leeds.ac.uk)

Abstract

Synoptic meteorology can have a significant influence on UK air quality. Cyclonic conditions lead to the dispersion of air pollutants away from source regions, while anticyclonic conditions lead to their accumulation over source regions. Meteorology also modifies atmospheric chemistry processes such as photolysis and wet deposition. Previous studies have shown a relationship between observed satellite tropospheric column NO_2 and synoptic meteorology in different seasons. Here, we test whether the UK Met Office Air Quality in the Unified Model (AQUM) can reproduce these observations and then use the model to explore the relative importance of various factors. We show that AQUM successfully captures the observed relationships, when sampled under the Lamb Weather Types, an objective classification of midday UK circulation patterns. By using a range of idealised NO_x-like tracers with different e-folding lifetimes, we show that under different synoptic regimes the NO_2 lifetime in AQUM is approximately 6 h in summer and 12 h in winter. The longer lifetime can explain why synoptic spatial column NO_2 variations are more significant in winter compared to summer, due to less NO_2 photochemical loss. We also show that cyclonic conditions have more seasonality in column NO_2 than anticyclonic conditions as they result in more extreme spatial departures from the wintertime seasonal average. Within a season (summer or winter) under different synoptic regimes, a large proportion of the spatial pattern in the UK column NO_2 field can be explained by the idealised model tracers, showing that transport is an important factor in governing the variability of UK air quality on seasonal synoptic timescales.

1 Introduction

Local air quality (AQ) can be influenced significantly by regional weather systems through the accumulation and dispersion of atmospheric pollutants over and away from source regions and populated areas. Local air quality can also be influenced by changes in atmospheric chemistry processes. For example, increased cloudiness will reduce photolysis

rates below cloud and increased precipitation can lead to enhanced removal of pollutants by wet deposition.

Many studies have used synoptic weather classifications to investigate the influence on AQ. These include objective classifications such as the Lamb Weather Type (LWT) and the North Atlantic Oscillation (NAO) Index. The LWTs are an objective description of the daily midday atmospheric circulation over the UK based on mean sea level pressure reanalysis data (Jones et al., 2013). The NAO Index is based on the pressure gradient between the Icelandic low and the Azores/Gibraltaran high pressure systems (Jones et al., 1997). In winter this pressure gradient has a significant influence on UK weather, where the positive phase can result in mild wet winters and the negative phase can lead to cold stable conditions (Osborn, 2006).

Previous studies including Demuzere et al. (2009); Tang et al. (2011); Lesniok et al. (2010) and McGregor and Bamzelis (1995) have used surface observations of air pollution to look at these AQ – regional weather relationships. Pope et al. (2014) and Thomas and Devasthale (2014) were two of the first studies to use earth observation (EO) of atmospheric pollutants, in combination with measures of synoptic weather, to investigate the influence of regional weather on AQ. Pope et al. (2014) used the LWTs and Ozone Monitoring Instrument (OMI) tropospheric column NO_2 between 2005 and 2011 (note that in the following we often refer to "tropospheric column NO_2" as "column NO_2"). They found that anticyclonic and cyclonic conditions lead to the accumulation and transport of air pollutants over and away from source regions, respectively. They also successfully detected the leeward transport of column NO_2 away from source regions under certain wind directions, similar to Beirle et al. (2011) and Hayn et al. (2009). These two studies used OMI column NO_2 and wind information to analyse NO_2 transport from the isolated megacity Riyadh, Saudi Arabia and Johannesburg, South Africa, respectively. Zhou et al. (2012) found significant impacts of wind speed and precipitation on OMI column NO_2 over western Europe. Savage et al. (2008) investigated the interannual variability (IAV) of satellite NO_2 columns over Europe, finding that meteorology influences NO_2 IAV more than emissions. Thomas and Devasthale (2014) found that Atmospheric Infrared Sounder (AIRS) CO at 500 hPa from 2002 to 2013

3

over the Nordic countries increased by 8, 4, 2.5 and 1 % under southeasterly winds, northwesterly winds, the positive phase of the NAO and anticyclonic conditions, respectively. The clearest conditions were under northeasterly winds and the negative phase of the NAO when cleaner Arctic air was transported into the Nordic region. When looking at the Global Ozone Monitoring Experiment (GOME) column NO_2 and the NAO, Eckhardt et al. (2003) found that significant positive phases lead to the reduction in column NO_2 over western Europe. However, Pope et al. (2014) did not find any clear evidence for this relationship.

This paper uses both satellite observations and the UK Met Office's operational Air Quality in the Unified Model (AQUM) to extend on the work of Pope et al. (2014). We investigate the differences in the air quality-synoptic weather relationships found by Pope et al. (2014) by attempting to quantify the dominant processes involved, for example, is atmospheric chemistry or weather more important in governing the links between synoptic meteorology and air quality in different seasons? First, we assess the ability of AQUM to simulate UK air quality under different synoptic regimes found in the OMI data. This is defined as "dynamical" model evaluation, i.e. assessing a model's ability to simulate changes in air quality stemming from changes in emissions and/or meteorology (Dennis et al., 2010). This follows the work by Pope et al. (2015) who used "operational" model evaluation, i.e. statistical analyses aimed at determining the agreement between the model and observations (Dennis et al., 2010), to perform the first evaluation of AQUM against satellite observations. Then, we use AQUM e-folding tracers with specified lifetimes designed to assess the impact of meteorology, emissions and chemistry on UK AQ.

The paper is structured as follows: Sect. 2 discusses the LWTs and OMI column NO_2 data. The model setup and application of OMI averaging kernels (AK) is discussed in Sect. 3. Section 4 shows our OMI/AQUM–LWT results for 2006–2010 and our conclusions are presented in Sect. 5.

4

2 Data

2.1 Lamb weather types

Lamb (1972) originally had a manual methodology of classifying the UK weather patterns but that has been superseded by automated methods. The objective (automated) LWTs,
[5] developed by Jones et al. (2013) based on the algorithm of Jenkinson and Collison (1977) and using the NCEP reanalyses midday mean sea level pressure data described by Kalnay et al. (1996), classify the atmospheric circulation patterns over the UK according to the wind direction and circulation type. The LWTs (Table 1) are grouped into three vorticity types (neutral vorticity, cyclonic and anticyclonic) and eight wind flow directions unless solely clas-
[10] sified as cyclonic or anticyclonic. The left column and top row of Table 1 show the grouped classifications used by Pope et al. (2014) to composite OMI column NO_2 data between 2005 and 2011. In this study we focus on 2006-2010 to match the AQUM simulation period, but only focus on seasonal cyclonic and anticyclonic conditions. Therefore, from here on in, references to "OMI-LWT" or "AQUM-LWT" comparisons relate to the analysis of OMI or
[15] AQUM tropospheric column NO_2 fields under seasonal cyclonic or anticyclonic conditions. For more information on the application of the LWTs to composite OMI and AQUM column NO_2 see Pope et al. (2014).

2.2 Satellite data

OMI is aboard NASA's EOS-Aura satellite and has an approximate UK daytime over-
[20] pass of 13:00 local time (LT). It is a nadir-viewing instrument with pixel sizes between 16–23 and 24–135 km along and across track, respectively, depending on the viewing zenith angle (Boersma et al., 2008). The tropospheric column NO_2 data used here is the DOMINO product version 2.0, which comes from the Tropospheric Emissions Monitoring Internet Service (TEMIS) (Boersma et al., 2011a, b) and is available from http:
[25] //www.temis.nl/airpollution/no2.html. We have binned NO_2 swath data from 01 January 2006 to 31 December 2010 onto a daily 13:00 LT $0.25° \times 0.25°$ grid between 43–63° N

and 20° W–20° E. All satellite retrievals were quality controlled, and retrievals/pixels with geometric cloud cover greater than 20 % and poor quality data flags (flag = −1 including retrievals affected by row anomalies and flagged by the Braak, 2010 algorithm) were removed. Several studies including Irie et al. (2008) and Boersma et al. (2008) have validated OMI column NO_2 against surface and aircraft measurements of tropospheric column NO_2 with good agreement within the OMI uncertainty ranges. Therefore, we have confidence in the OMI column NO_2 used in this study.

3 Air Quality in the Unified Model (AQUM)

3.1 Model setup

The AQUM domain covers approximately 45–60° N and 12° W–12° E, on a rotated grid, including the British Isles and part of continental Europe. The grid resolution is 0.11° × 0.11° in the horizontal and the model extends from the surface to 39 km on 38 levels. It has a coupled online tropospheric chemistry scheme, which uses the UK Chemistry and Aerosols (UKCA) subroutines. A complete description of this chemistry scheme, known as Regional Air Quality (RAQ), is available from the online Supplement of Savage et al. (2013). It includes 40 tracers, 18 non-advected species, 23 photolysis reactions and 115 gas-phase reactions. It also includes the heterogeneous reaction of N_2O_5 on aerosol as discussed by Pope et al. (2015).

For aerosols, AQUM uses the Coupled Large-scale Aerosol Simulator for Studies In Climate (CLASSIC) aerosol scheme. Aerosols are treated as an external mixture simulated in the bulk aerosol scheme. It contains six prognostic tropospheric aerosol types: ammonium sulphate, mineral dust, fossil fuel black carbon (FFBC), fossil fuel organic carbon (FFOC), biomass burning aerosols and ammonium nitrate. It also includes a fixed climatology for biogenic secondary organic aerosols (BSOA) and a diagnostic scheme for sea salt. For more details of the aerosol scheme see Bellouin et al. (2011).

6

Meteorological initial conditions and lateral boundary conditions (LBCs) come from the Met Office's operational global Unified Model (25×25 km) data. The chemical initial conditions come from AQUM's forecast for the previous day and the chemical LBCs are provided by the global Monitoring Atmospheric Composition and Climate (MACC) reanalyses (Inness et al., 2013). Pope et al. (2015) showed that for 2006, using the ECMWF GEMS (Global and regional Earth-system Monitoring using Satellite and in-situ data) reanalysis (Hollingsworth et al., 2008) LBCs provided more accurate forecasts than using the MACC LBCs. However, the GEMS LBCs are only available for 2006–2008. Therefore, we have used the MACC LBCs, which are available for the full period analysed here.

The model emissions were generated by merging three datasets: the National Atmospheric Emissions Inventory (NAEI) (1×1 km) for the UK, ENTEC (5×5 km) for the shipping lanes and European Monitoring and Evaluation Programme (EMEP) (50×50 km) for the rest of the model domain. NAEI NO_x emissions consist of point and area sources. Area sources include light industry, urban emissions and traffic, while elevated point sources are landfill, power stations, incinerators and refineries. Typically, the point source emissions are $100 \, \mathrm{g \, s^{-1}}$ in magnitude, while the area sources tend to be $10 \, \mathrm{g \, s^{-1}}$. The emissions are initially annual totals, however, the seasonal scaling factor from Visschedijk et al. (2007) is applied. See Pope et al. (2015) for more information. NO_x lightning emissions are parameterised based on model convection (O'Connor et al., 2014). AQUM does not include any soil NO_x sources, but large emissions from transport and industry in this region will dominate (Zhang et al., 2003).

AQUM was run for 5 years from 01 January 2006 to 31 December 2010. Five years provide a sufficient model data record to test the OMI column NO_2–LWT relationships. There are a few missing days for the 5 year simulation as the MACC LBCs do not exist over the full period (i.e. 4–6 June 2007 are missing).

As AQUM is a limited area NWP model, with meteorological boundary conditions from an operational NWP analysis and short (24 h) forecasts, the representation of large-scale weather systems via the LBCs is likely to be highly consistent with the NCEP reanalyses,

7

used to calculate the LWTs. Jones et al. (2014) also show high correlations between LWTs derived with NCEP reanalyses and those from another independent reanalysis (20CR).

We have sampled the AQUM surface pressure and winds under summer and winter anticyclonic and cyclonic conditions (Figure 1 & 2). In this study, summer ranges from April to September and winter is October-March. This is between 2007-2010 as u and v winds were unfortunately not saved for 2006. Under cyclonic conditions, the pressure anomalies from the seasonal average range between -10 to 0 hPa and -20 to 0 hPa in summer and winter, respectively. Under anticyclonic conditions, the summer and winter anomalies range between 0-10 and 0-20 hPa (Figure 1). These pressure anomalies are consistent with cyclonic and anticyclonic conditions. Under anticyclonic conditions, the circulation is clockwise and is stronger in winter (3-10 m/s - Figure 2d) than summer (2-8 m/s - Figure 2b). Both the cyclonic regimes have anticlockwise circulation with stronger flow in winter (5-12 m/s - Figure 2c) than summer (4-10 m/s - Figure 2a). We have also correlated the surface pressure spatial pattern from AQUM and NCEP, sampled under the seasonal synoptic regimes, using the Spearman's Rank Test (Figure 3). This yielded correlations of between 0.47-0.69 at the 99.9% significance level. These are significant correlations showing consistency between the AQUM and NCEP surface pressure data (the primary variable used to generate the LWTs). The most reliable method to examine the influence of meteorology on AQUM column NO_2 would be to apply the LWT algorithm used by Jones et al. (2013) on the AQUM pressure fields directly. However, as we have shown AQUM and NCEP to have consistent meteorological fields, it is simpler to directly sample the AQUM under the existing LWTs. Therefore, we choose to sample AQUM column NO_2 fields using the LWT classifications derived from the NCEP reanalysis in Table 1.

3.2 OMI averaging kernels

Since OMI retrievals of column NO_2 range in sensitivity with altitude, the OMI AKs must be applied to the model for representative comparisons. The OMI retrievals use the Differential Optical Absorption Spectroscopy (DOAS) technique and the AK is a column vector. Following Huijnen et al. (2010) and the OMI documentation (Boersma et al., 2011b), the AKs are

applied to the model as:

$$y = \boldsymbol{A} \cdot \boldsymbol{x} \tag{1}$$

where y is the total column, $\boldsymbol{A}$ is the AK and $\boldsymbol{x}$ is the vertical model profile. However, here the tropospheric column is needed:

$$y_{\text{trop}} = \boldsymbol{A}_{\text{trop}} \cdot \boldsymbol{x}_{\text{trop}} \tag{2}$$

where $\boldsymbol{A}_{\text{trop}}$ is:

$$\boldsymbol{A}_{\text{trop}} = \boldsymbol{A} \cdot \frac{\text{AMF}}{\text{AMF}_{\text{trop}}} \tag{3}$$

AMF is the atmospheric air mass factor and AMF_{trop} is the tropospheric air mass factor. Initially, the AQUM NO_2 profile is interpolated to the satellite pressure grid. The AKs are then applied to the NO_2 sub columns using Equation 2. The AQUM sub-columns are then summed up to the satellite tropopause level. For more information on OMI tropospheric column NO_2, we refer the reader to (Boersma et al., 2008) and for more information on the effect of OMI AKs on AQUM column NO_2 see Pope et al. (2015).

4 Results

4.1 OMI tropospheric column NO$_2$–LWT relationships: 2006–2010

As AQUM was run for 2006–2010, the OMI column NO_2–LWT analyses performed by Pope et al. (2014) are repeated for this time period to assess whether the synoptic weather – AQ relationships are consistent between the 7 year period presented in that study and the 5 years analysed here. Figures 4 and 5 show the influences of cyclonic and anticyclonic conditions in winter and summer on column NO_2 from OMI. Again, summer ranges from

9

April to September and winter is October–March. These extended seasons give more temporal sampling of OMI column NO_2 and better composites under the weather regimes. Under cyclonic conditions, column NO_2 is transported away from the source regions, while anticyclonic conditions aid its accumulation. Figure 5 highlights significant (95 % confidence level – based on the Wilcoxon Rank Test, Pirovano et al., 2012) anomalies of up to $\pm 5 \times 10^{15}$ molecules cm^{-2} over the North Sea and UK under cyclonic conditions. The reverse is found under anticyclonic conditions. The spatial extent of the anomalies is greatest in winter for both vorticity regimes. Therefore, there are no significant differences between the synoptic weather – air quality relationships based on the 5- and 7 year comparisons. Hence, the LWT–OMI 5 year comparisons act as the baseline for comparisons between AQUM column NO_2 and the LWTs.

This method does include some meteorological biases such as cloud cover and tropopause height under the synoptic regimes. As cyclonic conditions (unstable weather) are associated with more cloud cover than anticyclonic conditions (more clear-sky days for OMI to retrieve NO_2 on), the NO_2 composite sample size will be larger under anticyclonic conditions. However, as shown by Pope et al. (2014), this methodology of using the LWTs does involve sufficient satellite data to generate sensible column NO_2 composites under both vorticity regimes. The tropopause height will vary depending on atmospheric vorticity, but this information is accounted for in the retrieval process.

4.2 AQUM tropospheric column NO_2–LWT relationships

AQUM column NO_2, composited under the LWTs, displays similar patterns to OMI (Fig. 6). For this comparison, AQUM output has been co-located spatially and temporally with each OMI retrieval and the averaging kernel applied. In winter, under cyclonic conditions AQUM column NO_2 ranges between $10–13 \times 10^{15}$ molecules cm^{-2} over the UK and Benelux source regions (Fig. 6c). Over the western and eastern model domain, column NO_2 ranges between $0–4 \times 10^{15}$ molecules cm^{-2} and $5–8 \times 10^{15}$ molecules cm^{-2}, respectively. Under winter anticyclonic conditions column NO_2 over UK and Benelux source regions is $16–20 \times 10^{15}$ molecules cm^{-2} and the background column NO_2 ranges between

10

0–8 × 10^{15} molecules cm^{-2} (Fig. 6d). Larger background column NO$_2$ over the North Sea in Fig. 6c is indicative of cyclonic westerly transport off the UK mainland and the Benelux region, while larger source region column NO$_2$ in Fig. 6d highlights anticyclonic accumulation of NO$_2$.

5   When compared with OMI (Fig. 4c), AQUM sampled under the winter cyclonic conditions (Fig. 6c) shows transport of more column NO$_2$ over the North Sea ranging between 5–8 × 10^{15} molecules cm^{-2} and covering a larger spatial extent. Under anticyclonic conditions (Fig. 6d), AQUM column NO$_2$ is lower than OMI over the London and Benelux region by 2–3 × 10^{15} molecules cm^{-2}. However, AQUM column NO$_2$ is higher than OMI over northern

10   England by 2–3 × 10^{15} molecules cm^{-2}. The AQUM-OMI winter anticyclonic background column NO$_2$ is similar, ranging between 0–5 and 5–10 × 10^{15} molecules cm^{-2} over the sea and continental Europe, respectively.

Both OMI and AQUM show similar patterns in summer for both vorticity types, but with lower spatial extents than winter. Interestingly, the OMI cyclonic UK source region col-

15   umn NO$_2$ is larger in summer (8–10 × 10^{15} molecules cm^{-2} – Fig. 4a) than winter (6–8 × 10^{15} molecules cm^{-2} – Fig. 4c), but AQUM does not simulate this (Fig. 6a and c). AQUM summer cyclonic UK source region NO$_2$ ranges between 6–8 × 10^{15} molecules cm^{-2}, while in winter it is 10–12 × 10^{15} molecules cm^{-2}.

The AQUM and OMI transport and accumulation similarities and differences can be seen

20   in Figs. 5 and 7, which show anomalies of the composite averages calculated as differences with respect to the 5 year seasonal means. Under winter cyclonic conditions, both AQUM (Fig. 7c) and OMI (Fig. 5c) show significant negative and positive anomalies of similar magnitude over the UK and North Sea, respectively. Winter anticyclonic conditions lead to an accumulation of AQUM (Fig. 7d) and OMI (Fig. 5d) column NO$_2$ over UK and English

25   Channel, causing significant positive anomalies of 1–3 × 10^{15} molecules cm^{-2}. The summer AQUM (Figs. 7a and b) and OMI (Figs. 5a and b) synoptic-column NO$_2$ spatial patterns are similar in extent and magnitude. They are similar to the winter equivalents, but cover a smaller spatial extent. Therefore, on the regional scale, we can say that AQUM captures

the OMI column NO_2–LWT relationships with similar significant anomalies from the period average.

For a more complete dynamical model evaluation the differences between AQUM and OMI column NO_2 have been quantified. To compare the spatial extent of the anomaly fields from AQUM and OMI under the different seasonal weather regimes metrics such as correlation, slope of the linear regression and RMSE could be used, but these have limitations. Correlation only accounts for the spatial patterns of the anomalies and not the magnitude. Also, it does not account for the significance of the anomalies. Linear regression should indicate the best AQUM-OMI agreement when tending towards a $1:1$ fit. However, this metric does not account for anomaly significance either. RMSE does not always give a good indication of the error in the anomaly field magnitudes or in the spatial extent of the significant anomaly clusters. Here, we use the term "cluster" to represent a grouping of positive or negative significant anomalies. For instance, if an anomaly cluster for AQUM has a smaller spatial extent than OMI, the error magnitudes will be larger where the two are different, degrading the comparisons. Comparisons can also be degraded if the anomalies in AQUM and OMI are similar but offset slightly (e.g. should the model anomaly cluster be offset to the east by $0.5°$).

A more appropriate method to compare AQUM and OMI column NO_2 under the four regimes, which we do here, is to analyse both the spatial extent of the significant anomalies and their magnitude. For each of the seasonal synoptic regimes the number of significant positive and negative column NO_2 anomalies (pixels) were calculated. This represents the spatial extent of significance. The anomalies were grouped into separate counts of the positive and negative anomaly clusters as they show independent features across the model domain. To ascertain the magnitude of the anomaly clusters, the average positive and negative anomaly was calculated. This means that the spatial extent and size of the anomalies are both accounted for. We then define the cluster density to be the product of the respective cluster size (i.e. number of pixels) and its average anomaly magnitude giving:

$$\phi_\pm = \alpha_\pm \times \eta_\pm \tag{4}$$

12

where ϕ is the anomaly cluster density, α represents the size of the anomaly cluster, η is the average magnitude of the anomaly cluster and $\pm$ indicates if it is the positive or negative anomaly cluster density. The AQUM and OMI anomaly cluster densities were then compared using the fractional gross error (FGE). FGE is a normalised metric of the model's deviation from the observations which performs symmetrically with respect to under- and over-prediction, and is bounded by the values 0–2 (for more information see Savage et al., 2013; Pope et al., 2015). In this study's context, the FGE is represented by:

$$\text{FGE}_{\pm} = 2 \left| \frac{\phi_{\text{AQUM}_{\pm}} - \phi_{\text{OMI}_{\pm}}}{\phi_{\text{AQUM}_{\pm}} + \phi_{\text{OMI}_{\pm}}} \right| \tag{5}$$

In Fig. 8, the AQUM-OMI positive and negative FGEs for the four seasonal/synoptic cases are plotted against each other in red. The smaller the FGE, the closer the AQUM-OMI column NO_2 comparisons are under the seasonal synoptic regimes. A goal zone of $x = 0, y = 0$ would show that AQUM can accurately simulate the column NO_2–LWT relationships seen by OMI. However, this method only works if the anomaly clusters are in similar locations in the AQUM and OMI fields. From observation of Figs. 5 and 7, the anomaly dipole clusters cover the same regions in both datasets and spatial variances (R^2), discussed in more detail at the end of the section, show high associations between the two (i.e. the anomaly clusters are in similar locations). Therefore, we suggest that we can use this methodology to assess the skill of AQUM in simulating seasonal synoptic relationships seen in the OMI data, by looking at the size and magnitude of the anomaly clusters. In Fig. 8 we have added 4 arbitrary zones which indicate the closeness to the goal of $x = 0, y = 0$.

Summer cyclonic conditions give the best comparisons with positive and negative FGEs of approximately 0.4 and 0.45, respectively. This falls in Zone 1, closest to the (0,0) goal zone. Winter anticyclonic conditions have the next best agreement as the negative FGE shows small differences of under 0.1. Therefore, AQUM under these conditions can accurately represent the OMI negative anomaly pattern. However, the positive FGE is approximately 0.75 resulting in a comparison skill in Zone 2. The winter cyclonic conditions present FGE values of approximately 0.7 for both anomaly clusters falling into Zone 2 as well. Summer anticyclonic conditions show the poorest comparisons falling in Zone 4 with reasonable

13

agreement in the positive FGE of 0.4–0.5, but 1.5 in the negative FGE. This appears mostly to be a result of the smaller magnitude and extent of the negative anomalies in the proximity of the North Sea within the model, where they are significant for much fewer pixels (Fig. 7b) than in the observations (Fig. 5b).

In Table 2 we justify using our approach of using the anomaly clusters and FGE when compared with other statistical metrics. The table highlights the order in which AQUM most successfully reproduces the OMI column NO_2 anomalies when sampled under the seasonal synoptic regimes. Like the correlation and RMSE, our method has summer cyclonic, winter anticyclonic and winter cyclonic in the same order. However, summer anticyclonic has the worst comparisons using our method. This is because in the anomaly fields (Figure 7), our method shows AQUM does not simulate significant negative biases whereas the other metrics show the best apparent agreement. This justifies our new method as it takes into account the significance of the anomalies, unlike the other metrics.

The spatial variance (R^2) between AQUM and OMI column NO_2 anomalies (both significant and non-significant) is 0.70, 0.61, 0.68 and 0.59 for summer anticyclonic, summer cyclonic, winter anticyclonic and winter cyclonic conditions, respectively. This represents the proportion of spatial variability in OMI column NO_2 anomalies captured by the AQUM column NO_2 anomalies for each seasonal synoptic regime. For all the seasonal regimes, the association between the AQUM and OMI anomaly fields is significant large, with peak associations in the anticyclonic comparisons. As the associations are strong, the anomaly spatial patterns are located in similar locations, as can be seen in Figures 5 and 7. Therefore, this provides us with further confidence to use the methodology discussed in Equation 5 to analyse the size and spread of the significant anomalies for each seasonal synoptic regime. Interestingly, even though AQUM does not simulate the significant negative anomalies over the North Sea (worst comparisons in Fig. 8) under summer anticyclonic conditions (Fig. 7b), it does capture the spatial variability in the OMI anomalies (Fig. 5b) better than under the other regimes. However, the two metrics were used to look at different objectives. As stated above, the R^2 values show the spatial agreement between the AQUM and OMI

14

anomaly fields, while the cluster and FGE analysis focus on the significance and magnitude of the anomaly clusters.

4.3 AQUM tropospheric column tracer–LWT relationships

Section 4.2 has shown that AQUM successfully reproduces the relationships seen by OMI
5 column NO_2 when sampled under the LWTs. Therefore, AQUM can be used as a tool to diagnose the influence of meteorology and chemistry on the distribution of NO_2 under the seasonal weather regimes. Here idealised tracers are introduced into AQUM with e-folding lifetimes of 1, 3, 6, 12, 24 and 48 h. They are emitted with the same loading and over the same locations as the model NO_x. This method of using e-folding tracers has been applied
10 in inverse modelling of NO_x emissions from satellite data. For example, Richter et al. (2004) used SCIAMACHY column NO_2 measurements and simple approximations of NO_x loss (i.e. a fixed lifetime of NO_x) to estimate shipping emissions over the Red Sea. These idealised tracers will indicate the importance of transport and atmospheric chemistry governing the relationships between column NO_2 and seasonal synoptic weather. If transport is the main
15 factor governing the air quality distribution under the different synoptic regimes, then a fixed lifetime tracer would have similar anomaly fields to NO_2. On the other hand, if changes in chemistry are driving or significantly contributing to the different regime anomalies, then a certain fixed lifetime tracer would be unable to capture the observed differences. Therefore, depending on which of the tracers with different lifetimes results in anomaly fields
20 most similar to the AQUM column NO_2 anomalies, for winter and summer cyclonic and anticyclonic regimes, the relative importance of the processes can be determined and an approximation for the model lifetime of NO_2. Beirle et al. (2003) used GOME tropospheric column NO_2 over Germany to estimate a summer life-time of approximately 6 hours and a winter life-time of 18-24 hours.

25 As the chemistry of NO_x is complex, with non-linear relations via ozone, diurnal cycles and varying emissions, a simple e-folding tracer will never truly match the NO_2 distribution. However, this approach is less complex than investigating chemical budgets and wind fields, which are not available from the AQUM for this study. Also, the direct lifetime of NO_2

15

cannot be determined as fluxes through the model boundaries are likely a strong sink or source under different conditions. Therefore, the tracers will indicate transport and chemical representation to a first-order approximation, and can be used to answer questions such as "Does the use of tracers support the well-known fact that the chemical lifetime of NO_2 is shorter in summer than in winter?; if so does synoptic meteorology have a smaller effect on NO_2 columns in summer than in winter?".

The same method of compositing AQUM column NO_2 has been applied to the e-folding tracer columns. The tracer anomalies under the seasonal synoptic conditions are shown in Figs. 9 (summer) and 10 (winter) with OMI AKs applied. The tracers successfully reproduce the spatial patterns seen in the AQUM and OMI column NO_2 sampled under the different seasonal synoptic regimes. However, the area size of the tracer anomalies (both the negative and positive clusters) are a function of the tracer lifetime. In the case of the tracers with 1 and 3 h lifetimes ($tracer_1$ and $tracer_3$), the anomaly cluster areas are small. The short lifetime means that there is less column tracer to be accumulated or transported under anticyclonic or cyclonic regimes. With the longer lifetimes, $tracer_{24\ and\ 48}$, these anomaly cluster areas cover a larger proportion of the domain. This pattern can be seen in Fig. 11, where as the lifetime increases from 1 to 48 h, the cluster size of significant pixels (positive and negative totals combined) increases from a fraction of 0.0 to 0.3–0.5 (depending on seasonal synoptic regime). This clearly shows that the lifetime of the tracer is important and has an impact on the spatial pattern (area size) of the tracer column anomalies.

The summer and winter anticyclonic curves in Fig. 11 are very similar reaching approximately 0.35 for $tracer_{48}$. This suggests that under anticyclonic conditions differences in meteorology between the two seasons have relatively little impact on the area of significant tracer columns. Thus the chemistry is playing an important role in the summer to winter differences in the spatial distributions. However, under cyclonic conditions, the winter anomalies are somewhat larger than the summer ones, reaching approximately 0.51 and 0.47, respectively, for $tracer_{48}$. Here differences in meteorology between summer and winter are playing a more active role suggesting that winter cyclonic systems are more intense than summer equivalents. From Figure 2 the AQUM winter cyclonic wind speed ranges be-

16

tween 5–12 m/s. In summer, the equivalent summer cyclonic wind speed ranges between 4–10 m/s. Therefore, the cyclonic wind speeds are stronger in winter. Thus, the stronger transport in winter probably explains the difference in the cyclonic curves in Figure 11.

The analysis performed previously for the FGEs of the AQUM and OMI column NO_2

5 anomaly cluster densities (Fig 8) was repeated for the FGEs of the AQUM column NO_2 and tracer column anomaly cluster densities in Fig 12. Therefore, in Equation 5, $\phi_{AQUM_{\pm}}$ has been replaced with $\phi_{tracer_{\pm}}$ and $\phi_{OMI_{\pm}}$ has been replaced with $\phi_{AQUM_{\pm}}$. The aim is to find which tracer lifetimes most accurately represent the NO_2 lifetime under the seasonal synoptic regimes. Overall, tracers$_{1,\ 3\ \text{and}\ 48}$ have the least accurate lifetimes with skill comparisons

10 in Zone 4, because the domain coverage of the tracer anomalies is either too small or too large (the winter tracer$_{48}$ regimes fall into Zone 3). The most accurate tracer lifetime for summer cyclonic and anticyclonic regimes is tracer$_6$, with FGE values between 0.3 (Zone 1) and 0.6–0.7 (Zone 2), respectively. The winter cyclonic and anticyclonic regimes are most accurately represented by tracer$_{12}$; both of them fall into Zone 1 with FGE values lower than 0.4.

15 This is more consistent with chemical processes in summer than winter acting as a loss of NO_2. To verify this result, the AQUM column NO_2 significant anomaly domain fraction was calculated at 0.02, 0.04, 0.07 and 0.09 for summer anticyclonic, summer cyclonic, winter anticyclonic and winter cyclonic conditions, respectively. Reading across to the respective tracer profiles in Figure 11, the approximate NO_2 lifetimes are 6.0, 4.5, 11.0 and 7.0 hours,

20 respectively. This supports the tracer results in that summer NO_2 lifetimes are shorter than that of winter, similar to the result of Beirle et al. (2003). It should be noted though that this approach does not take into account the magnitude of the anomalies.

Having found the best representations of the seasonal synoptic regimes' lifetimes, the respective tracer anomaly fields were correlated against the AQUM column NO_2 anoma-

25 lies. Since the tracer lifetime was fixed, the variance between the tracer fields and the column NO_2 represents the proportion of meteorological variability in the spatial pattern of the anomalies within the season (the emissions for each seasonal synoptic regime NO_2 – tracer comparison are equal). The variances (R^2) are 0.92, 0.87, 0.80 and 0.75 for the summer anticyclonic, summer cyclonic, winter anticyclonic and winter cyclonic conditions,

respectively. Therefore, a large proportion of the seasonal variability in the spatial patterns, under the seasonal synoptic regimes, is explained by the meteorology (e.g. transport) and the remaining variability is due to the chemistry and emissions.

5 Conclusions

5 The LWTs (cyclonic and anticyclonic) - OMI tropospheric column NO_2 relationships discussed by Pope et al. (2014) for a 7-year period have been analysed for the 2006-2010 period simulated by AQUM in order to investigate the model's ability to capture the impact of synoptic weather on tropospheric column NO_2.

AQUM column NO_2, composited in the same way as OMI data by using the LWTs directly,
10 successfully captured the OMI column NO_2 anomalies for cyclonic and anticyclonic LWT conditions. Under anticyclonic conditions, AQUM column NO_2 accumulates over the source regions, while it is transported away under cyclonic conditions. This also shows that the representation of weather systems through the model LBCs is sufficiently consistent with the NCEP reanalyses that the LWTs derived from NCEP can be used to investigate the
15 influence of synoptic weather regimes on air quality.

To determine which processes are important in driving these relationships, idealised tracers were introduced into the model using the NO_x emission sources and selected lifetimes ranging from 1 to 48 h. The tracers reproduce the AQUM column NO_2 anomaly fields under the different seasonal synoptic regimes, but the relationships found depend heavily on
20 the lifetime. A 1 h lifetime was clearly too short and a 48 h lifetime clearly too long, resulting in smaller/larger anomaly patterns when compared with the model column NO_2. The most representative tracer lifetimes are 6 h in summer and 12 h in winter, which is consistent with enhanced photochemistry in summer. The variance (R^2) between the most representative tracer lifetimes for the seasonal synoptic regimes and the corresponding AQUM
25 column NO_2 spatial anomaly fields were calculated. This resulted in R^2 values ranging between 0.75 and 0.92. Therefore, within seasons (i.e. summer and winter), under the synoptic regimes, a large proportion of the spatial pattern in the UK column NO_2 fields can be

18

explained by these tracers, suggesting that transport is a significant factor in governing the variability of UK air quality on seasonal synoptic timescales. We also show that cyclonic conditions have more seasonality than anticyclonic conditions as winter cyclonic conditions result in more extreme spatial column NO_2 distributions from the seasonal average.

This study shows that to a first-order approximation atmospheric chemistry is, as expected, more influential in summer than in winter. During summer the NO_2 lifetime decreases due to enhanced NO_2 photolysis and OH chemistry, which explains the less spatially significant synoptic weather-air pollution relationships detected for that season in OMI column NO_2 (Pope et al., 2014). This work also shows that the Met Office AQUM can reproduce the large-scale accumulation of tropospheric column NO_2 over the UK under anticyclonic conditions.

As follow on work from this study, we intend to perform a sensitivity analysis of different AQUM production and loss processes of NO_2 to determine the governing factors on the distribution of column NO_2.

References

Beirle, S., Boersma, K. F., Platt, U., Lawrence, M. G., and Wagner, T.: Megacity emissions and lifetimes of nitrogen oxides probed from space, Science, 333, 1737–1739, doi:10.1126/science.1207824, 2011.

Beirle, S., Platt, U., Wenig, M., and Wagner, T.: Weekly cycle of NO_2 by GOME measurements: a signature of anthropogenic sources, Atmospheric Chemistry and Physics, 3, 2225–2232, doi:, 2003.

Bellouin, N., Rae, J., Jones, A., Johnson, C., Haywood, J., and Boucher, O.: Aerosol forcing in the Climate Model Intercomparison Project (CMIP5) simulations by HadGEM2-ES and the role of ammonium nitrate, J. Geophys. Res.-Atmos., 116, D20206, doi:10.1029/2011JD016074, 2011.

Boersma, K., Jacob, D., Bucsela, E., Perring, A., Dirksen, R., van der A, R., Yantosca, R., Park, R., Wenig, M., Bertram, T., and Cohen, R.: Validation of OMI tropospheric NO_2 observations during INTEX-B and application to constrain emissions over the eastern United States and Mexico, Atmos. Environ., 42, 4480–4497, doi:10.1016/j.atmosenv.2008.02.004, 2008.

Boersma, K. F., Eskes, H. J., Dirksen, R. J., van der A, R. J., Veefkind, J. P., Stammes, P., Huijnen, V., Kleipool, Q. L., Sneep, M., Claas, J., Leitão, J., Richter, A., Zhou, Y., and Brunner, D.: An improved tropospheric NO_2 column retrieval algorithm for the ozone monitoring instrument, Atmos. Meas. Tech., 4, 1905–1928, doi:10.5194/amt-4-1905-2011, 2011a.

Boersma, K., Braak, R., and van der A, R.: Dutch OMI NO_2 (DOMINO) data product v2.0, Tropospheric Emissions Monitoring Internet Service on-line documentation, available at: http://www.temis.nl/docs/OMI_NO2_HE5_2.0_2011.pdf (last access: January 2015), 2011b.

Braak, R.: Row Anomaly Flagging Rules Lookup Table, KNMI Technical Document TN-OMIE-KNMI-950, KMNI, De Bilt, the Netherlands, 2010.

Demuzere, M., Trigo, R. M., Vila-Guerau de Arellano, J., and van Lipzig, N. P. M.: The impact of weather and atmospheric circulation on O_3 and PM_{10} levels at a rural mid-latitude site, Atmos. Chem. Phys., 9, 2695–2714, doi:10.5194/acp-9-2695-2009, 2009.

Dennis, R., Fox, T., Fuentes, M., Gilliland, A., Hanna, S., Hogrefe, C., Irwin, J., Rao, S., Scheffe, R., Schere, K., Steyn, D., and Venkatram, A.: A framework for evaluating regional-scale numerical photochemical modelling systems, Environ. Fluid Mech., 10, 471–489, doi:10.1007/s10652-009-9163-2, 2010.

Eckhardt, S., Stohl, A., Beirle, S., Spichtinger, N., James, P., Forster, C., Junker, C., Wagner, T., Platt, U., and Jennings, S. G.: The North Atlantic Oscillation controls air pollution transport to the Arctic, Atmos. Chem. Phys., 3, 1769–1778, doi:10.5194/acp-3-1769-2003, 2003.

Hayn, M., Beirle, S., Hamprecht, F. A., Platt, U., Menze, B. H., and Wagner, T.: Analysing spatio-temporal patterns of the global NO_2-distribution retrieved from GOME satellite observations using a generalized additive model, Atmos. Chem. Phys., 9, 6459–6477, doi:10.5194/acp-9-6459-2009, 2009.

Hollingsworth, A., Engelen, R., Benedetti, A., Dethof, A., Flemming, J., Kaiser, J., Morcrette, J., Simmons, A., Textor, C., Boucher, O., Chevallier, F., Rayner, P., Elbern, H., Eskes, H., Granier, C., Peuch, V.-H., Rouil, L., and Schultz, M. G.: Towards a monitoring and forecasting system for atmospheric composition: the GEMS project, B. Am. Meteorol. Soc., 89, 1147–1164, 2008.

Huijnen, V., Eskes, H. J., Poupkou, A., Elbern, H., Boersma, K. F., Foret, G., Sofiev, M., Valdebenito, A., Flemming, J., Stein, O., Gross, A., Robertson, L., D'Isidoro, M., Kioutsioukis, I., Friese, E.,

Amstrup, B., Bergstrom, R., Strunk, A., Vira, J., Zyryanov, D., Maurizi, A., Melas, D., Peuch, V.-H., and Zerefos, C.: Comparison of OMI NO_2 tropospheric columns with an ensemble of global and European regional air quality models, Atmos. Chem. Phys., 10, 3273–3296, doi:10.5194/acp-10-3273-2010, 2010.

Inness, A., Baier, F., Benedetti, A., Bouarar, I., Chabrillat, S., Clark, H., Clerbaux, C., Coheur, P., Engelen, R. J., Errera, Q., Flemming, J., George, M., Granier, C., Hadji-Lazaro, J., Huijnen, V., Hurtmans, D., Jones, L., Kaiser, J. W., Kapsomenakis, J., Lefever, K., Leitão, J., Razinger, M., Richter, A., Schultz, M. G., Simmons, A. J., Suttie, M., Stein, O., Thépaut, J.-N., Thouret, V., Vrekoussis, M., Zerefos, C., and the MACC team: The MACC reanalysis: an 8 yr data set of atmospheric composition, Atmos. Chem. Phys., 13, 4073–4109, doi:10.5194/acp-13-4073-2013, 2013.

Irie, H., Kanaya, Y., Akimoto, H., Tanimoto, H., Wang, Z., Gleason, J. F., and Bucsela, E. J.: Validation of OMI tropospheric NO_2 column data using MAX-DOAS measurements deep inside the North China Plain in June 2006: Mount Tai Experiment 2006, Atmos. Chem. Phys., 8, 6577–6586, doi:10.5194/acp-8-6577-2008, 2008.

Jenkinson, A. and Collison, F.: An initial climatology of gales over the North Sea, in: Synoptic Climatology Branch Memorandum No. 62, Meteorological Office, Bracknell, 1977.

Jones, P. D., Jonsson, T., and Wheeler, D.: Extension to the North Atlantic oscillation using early instrumental pressure observations from Gibraltar and south-west Iceland, Int. J. Climatol., 17, 1433–1450, doi:10.1002/(SICI)1097-0088(19971115)17:13<1433::AID-JOC203>3.0.CO;2-P, 1997.

Jones, P. D., Harpham, C., and Briffa, K. R.: Lamb weather types derived from reanalysis products, Int. J. Climatol., 33, 1129–1139, doi:10.1002/joc.3498, 2013.

Jones, P. D., Osborn, T. J., Harpham, C., and Briffa, K. R.: The development of Lamb weather types: from subjective analysis of weather charts to objective approaches using reanalyses, Weather, 69, 128–132, doi:10.1002/wea.2255, 2014.

Kalnay, E., Kanamitsuand, M., Kistler, R., Collins, W., Deaven, D., Gandin, L., Iredell, M., Saha, S., White, G., Wollen, J., Zhu, Y., Chelliah, M., Ebisuzaki, W., Higgins, W., Janowiak, J., Mo, K., Ropelewski, C., Wang, J., Leetmaa, A., Reynolds, R., Jenne, R., and Joseph, D.: The NCEP/NCAR 40 year reanalysis project, B. Am. Meteorol. Soc., 77, 437–471, 1996.

Lamb, H.: British Isles weather types and a register of daily sequence of circulation patterns, 1861–1971, in: Geophysical Memoir, HMSO, London, 116, 85, 1972.

Lesniok, M., Malarzewski, L., and Niedzwiedz, T.: Classification of circulation types for Southern Poland with an application to air pollution concentration in Upper Silesia, Phys. Chem. Earth, 35, 516–522, doi:10.1016/j.pce.2009.11.006, 2010.

McGregor, G. and Bamzelis, D.: Synoptic typing and its application to the investigation of weather air pollution relationships, Birmingham, United Kingdom, Theor. Appl. Climatol., 51, 223–236, doi:10.1007/BF00867281, 1995.

O'Connor, F. M., Johnson, C. E., Morgenstern, O., Abraham, N. L., Braesicke, P., Dalvi, M., Folberth, G. A., Sanderson, M. G., Telford, P. J., Voulgarakis, A., Young, P. J., Zeng, G., Collins, W. J., and Pyle, J. A.: Evaluation of the new UKCA climate-composition model – Part 2: The Troposphere, Geosci. Model Dev., 7, 41–91, doi:10.5194/gmd-7-41-2014, 2014.

Osborn, T. J.: Recent variations in the winter North Atlantic Oscillation, Weather, 61, 353–355, doi:10.1256/wea.190.06, 2006.

Pirovano, G., Balzarini, A., Bessagnet, B., Emery, C., Kallos, G., Meleux, F., Mitsakou, C., Nopmongcol, U., Riva, G., and Yarwood, G.: Investigating impacts of chemistry and transport model formulation on model performance at European scale, Atmos. Environ., 53, 93–109, doi:10.1016/j.atmosenv.2011.12.052, 2012.

Pope, R., Savage, N., Chipperfield, M., Arnold, S., and Osborn, T.: The influence of synoptic weather regimes on UK air quality: analysis of satellite column NO_2, Atmos. Sci. Lett., 15, 211–217, doi:10.1002/asl2.492, 2014.

Pope, R., Chipperfield, M., Savage, N., Ordóñez, C., Neal, L., Lee, L., Dhomse, S., Richards, N., and Keslake, T.: Evaluation of a regional air quality model using satellite column NO_2: treatment of observation errors and model boundary conditions and emissions, Atmos. Chem. Phys., 15, 5611-5626, doi:10.5194/acp-15-5611-2015, 2015.

Richter, A., Eyring, V., Burrows, J. P., Bovensmann, H., Lauer, A., Sierk, B., and Crutzen, P. J.: Satellite measurements of NO_2 from international shipping emissions, Geophys. Res. Lett., 31, L23110, doi:10.1029/2004GL020822, 2004.

Savage, N. H., Pyle, J. A., Braesicke, P., Wittrock, F., Richter, A., Nüß, H., Burrows, J. P., Schultz, M. G., Pulles, T., and van Het Bolscher, M.: The sensitivity of Western European NO_2 columns to interannual variability of meteorology and emissions: a model-GOME study, Atmos. Sci. Lett., 9, 182–188, 2008.

Savage, N. H., Agnew, P., Davis, L. S., Ordóñez, C., Thorpe, R., Johnson, C. E., O'Connor, F. M., and Dalvi, M.: Air quality modelling using the Met Office Unified Model (AQUM OS24-26): model

description and initial evaluation, Geosci. Model Dev., 6, 353–372, doi:10.5194/gmd-6-353-2013, 2013.

Tang, L., Rayner, D., and Haeger-Eugensson, M.: Have meteorological conditions reduced NO_2 concentrations from local emission sources in Gothenburg?, Water Air Soil Poll., 221, 275–286, doi:10.1007/s11270-011-0789-6, 2011.

Thomas, M. A. and Devasthale, A.: Sensitivity of free tropospheric carbon monoxide to atmospheric weather states and their persistency: an observational assessment over the Nordic countries, Atmos. Chem. Phys., 14, 11545–11555, doi:10.5194/acp-14-11545-2014, 2014.

Visschedijk, A., Zanveld, P., and van der Gon, H.: A high resolution gridded European emission database for the EU integrated project GEMS, TNO report 2007-A-R0233/B, 2007.

Zhang, R., Tie, X., and Bond, D.: Impacts of anthropogenic and natural NO_x sources over the US on tropospheric chemistry, PNAS, 100, 1505-1509, 2003.

Zhou, Y., Brunner, D., Hueglin, C., Henne, S., and Staehelin, J.: Changes in OMI tropospheric NO_2 columns over Europe from 2004 to 2009 and the influence of meteorological variability, Atmos. Environ., 46, 482–495, doi:10.1016/j.atmosenv.2011.09.024, 2012.

Table 1. The non-bold elements show the 27 basic Lamb Weather Types with their number coding. LWTs also include -1 (unclassified) and -9 (non-existent day). Pope et al. (2014) grouped the LWTs into 3 circulation types and 8 wind directions, as indicated in bold characters by the outer row and column. However, in this study we focus on the cyclonic and anticyclonic conditions.

This Work	Anticyclonic	Neutral Vorticity	Cyclonic
	0 A		20 C
North-easterly	1 ANE	11 NE	21 CNE
Easterly	2 AE	12 E	22 CE
South-easterly	3 ASE	13 SE	23 CSE
Southerly	4 AS	14 S	24 CS
South-westerly	5 ASW	15 SW	25 CSW
Westerly	6 AW	16 W	26 CW
North-westerly	7 ANW	17 NW	27 CNW
Northerly	8 AN	18 N	28 CN

Table 2. Highlights the skill rank of the seasonal synoptic regimes for which AQUM can simulate column NO_2 when compared with OMI column NO_2 using correlation, slope-of-regression, RMSE and the method proposed here. 1: Best AQUM-OMI agreement, 4: Worst AQUM-OMI agreement.

Rank	Correlation	Regression	RMSE	New Method
1	Summer Anticyclonic	Summer Anticyclonic	Summer Anticyclonic	Summer Cyclonic
2	Summer Cyclonic	Summer Cyclonic	Summer Cyclonic	Winter Anticyclonic
3	Winter Anticyclonic	Winter Cyclonic	Winter Anticyclonic	Winter Cyclonic
4	Winter Cyclonic	Winter Anticyclonic	Winter Cyclonic	Summer Anticyclonic
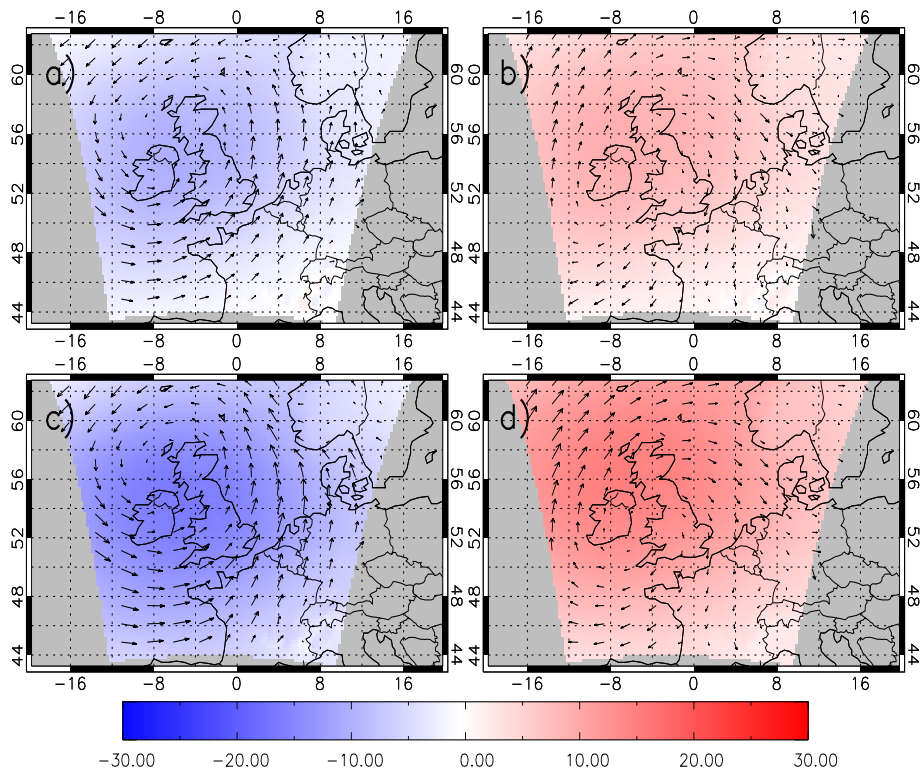
Figure 1. AQUM pressure anomalies (hPa) relative to the seasonal average (2007-2010) with the wind circulation over plotted. a) summer cyclonic, b) summer anticyclonic, c) winter cyclonic and d) winter anticyclonic, all derived from the Lamb Weather Types.
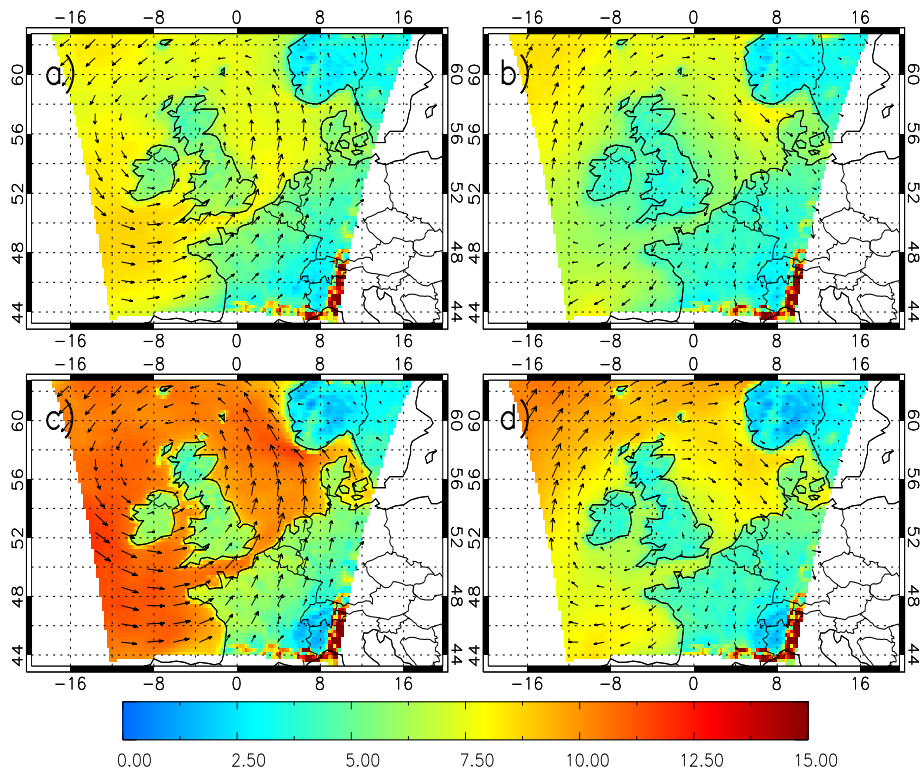
Figure 2. AQUM wind speed (m/s) for 2007-2010 with the wind circulation over plotted. a) summer cyclonic, b) summer anticyclonic, c) winter cyclonic and d) winter anticyclonic, all derived from the Lamb Weather Types.
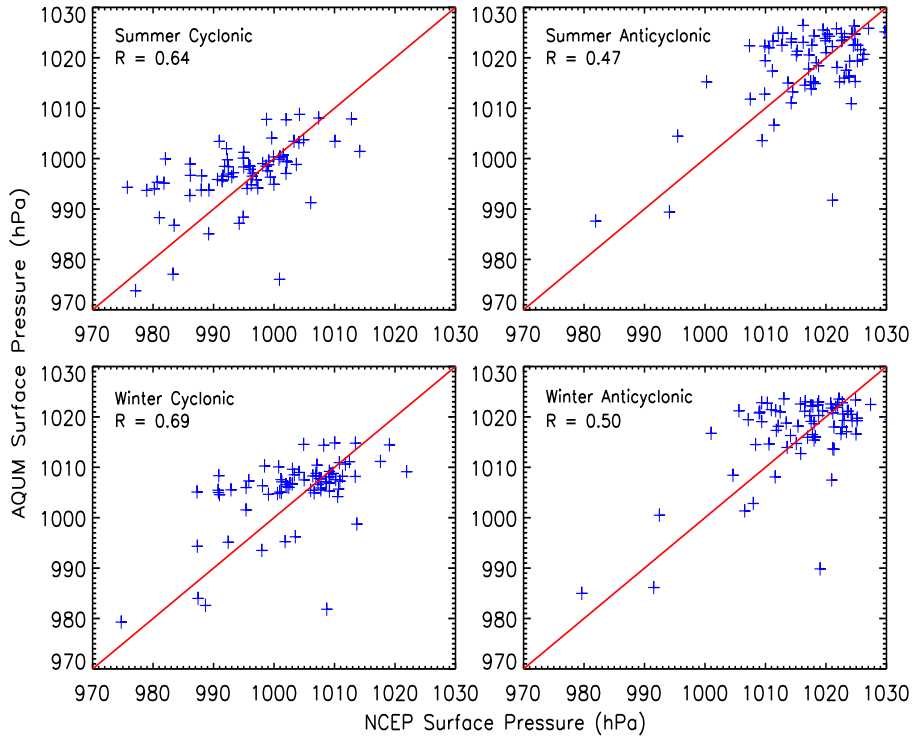
Figure 3. AQUM surface pressure vs. NCEP surface pressure (2006-2010), both composited under summer and winter cyclonic and anticyclonic conditions. The correlations are based on Spearman's Rank with a significance level of $p < 0.001$.
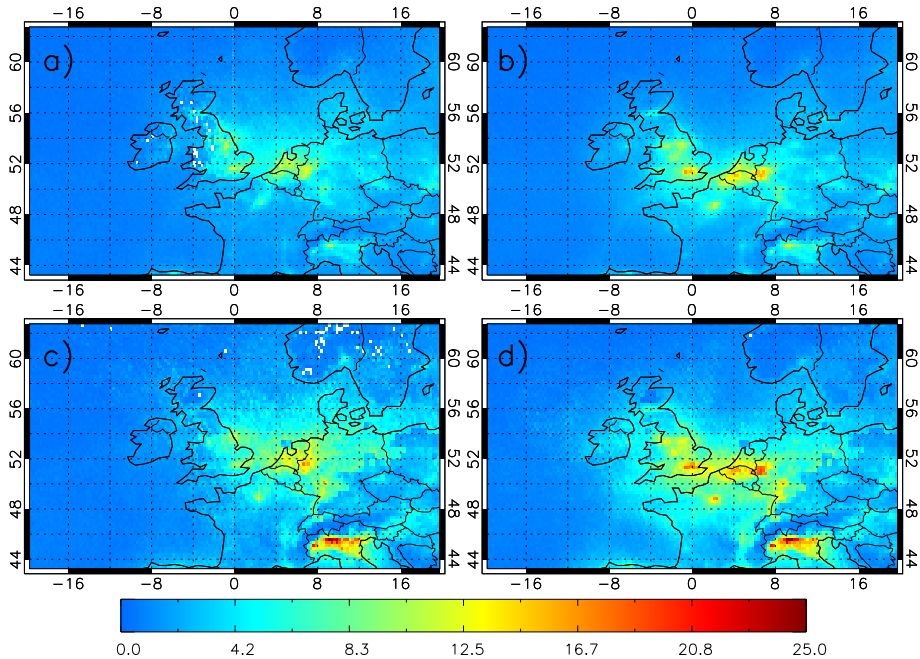
Figure 4. Composites of OMI tropospheric column NO$_2$ (10^{15} molecules cm^{-2}) for **(a)** summer cyclonic, **(b)** summer anticyclonic, **(c)** winter cyclonic and **(d)** winter anticyclonic conditions during 2006–2010.
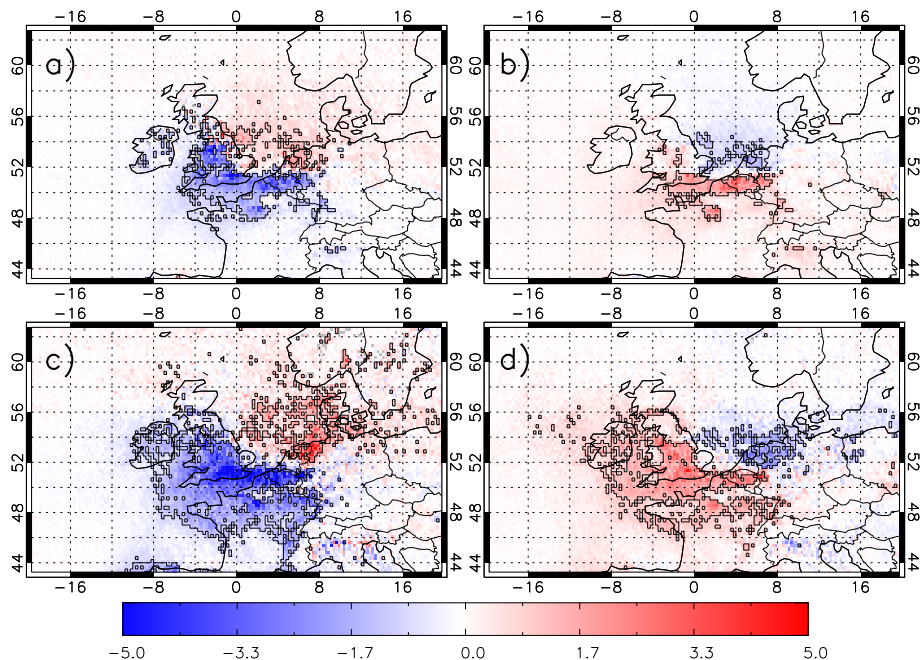
Figure 5. Anomalies of OMI tropospheric column NO_2 composites (calculated as the deviations with respect to the seasonal 5 year averages, 10^{15} molecules cm^{-2}) for **(a)** summer cyclonic, **(b)** summer anticyclonic, **(c)** winter cyclonic and **(d)** winter anticyclonic conditions. Black boxes indicate where the anomalies are statistically significant at the 95 % level.
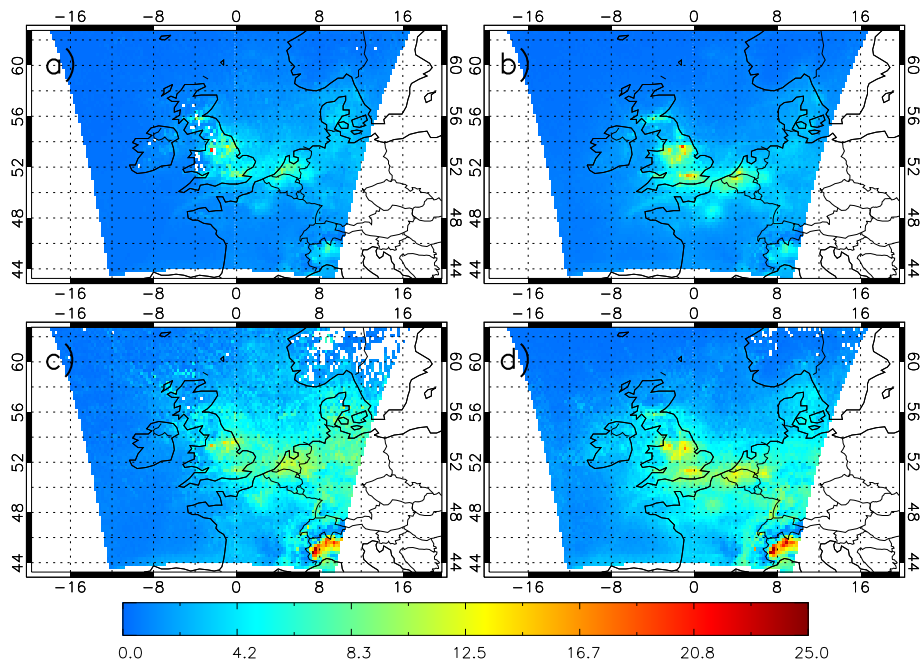
Figure 6. Composites of AQUM tropospheric column NO_2 (10^{15} molecules cm^{-2}) for **(a)** summer cyclonic, **(b)** summer anticyclonic, **(c)** winter cyclonic and **(d)** winter anticyclonic conditions (OMI AKs applied) during 2006–2010.
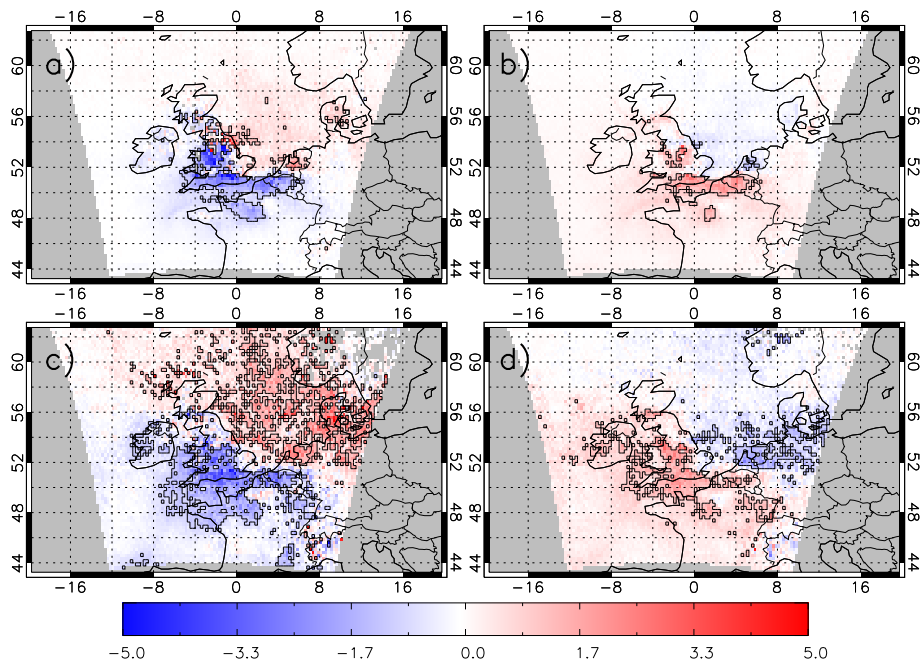
Figure 7. Anomalies of AQUM tropospheric column NO_2 composites (calculated as the deviations with respect to the seasonal 5 year averages, 10^{15} molecules cm^{-2}) for **(a)** summer cyclonic, **(b)** summer anticyclonic, **(c)** winter cyclonic and **(d)** winter anticyclonic conditions (OMI AKs applied).

32
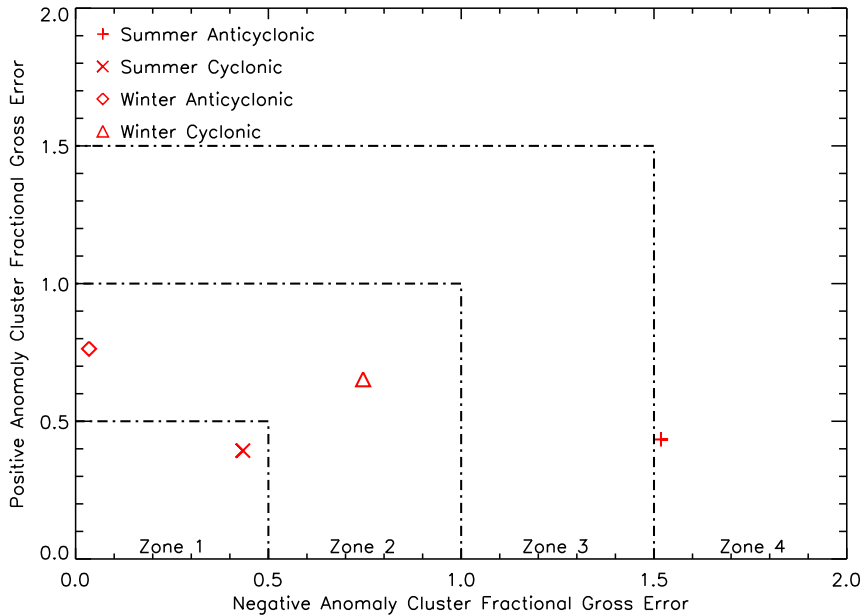
Figure 8. The fractional gross error of the AQUM-OMI positive and negative anomaly cluster densities are plotted against each other for different seasonal synoptic regimes. The best agreement between AQUM-OMI column NO_2 is at the goal zone ($x = 0, y = 0$) showing no error. Zones 1–4 represent areas of skill between 0.0–0.5, 0.5–1.0, 1.0–1.5 and 1.5–2.0. The lower the zone, the better the comparison is.
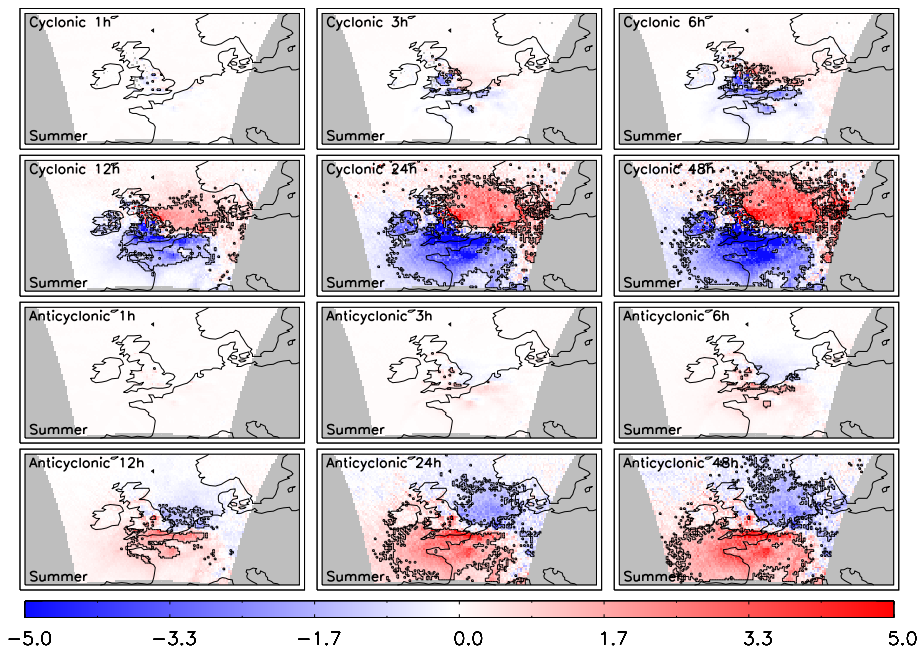
Figure 9. Summer AQUM column tracer anomalies (10^{15} molecules cm^{-2}) with different lifetimes for cyclonic and anticyclonic conditions (OMI AKs applied).
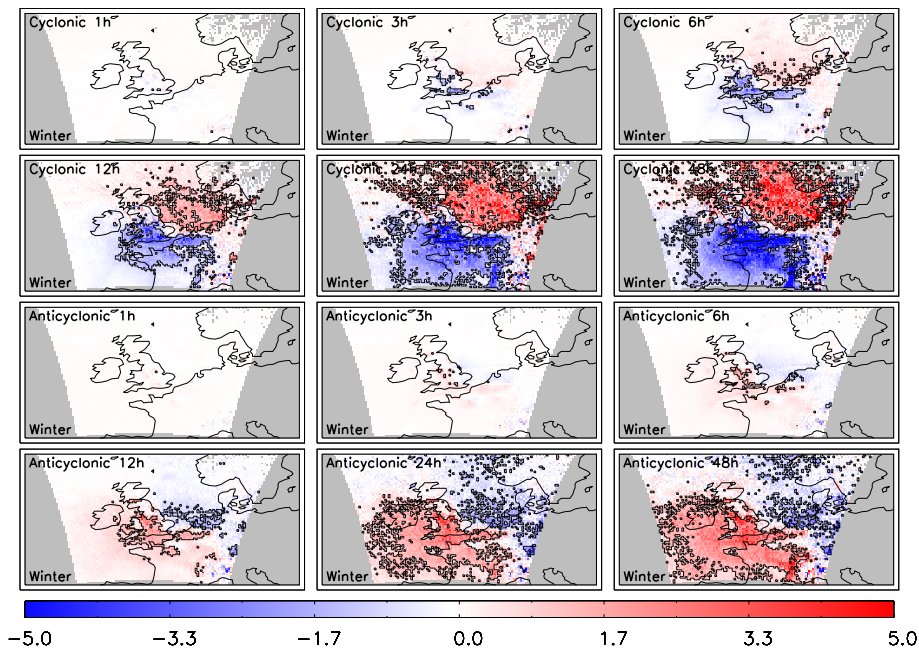
Figure 10. Winter AQUM column tracer anomalies (10^{15} molecules cm^{-2}) with different lifetimes for cyclonic and anticyclonic conditions (OMI AKs applied).
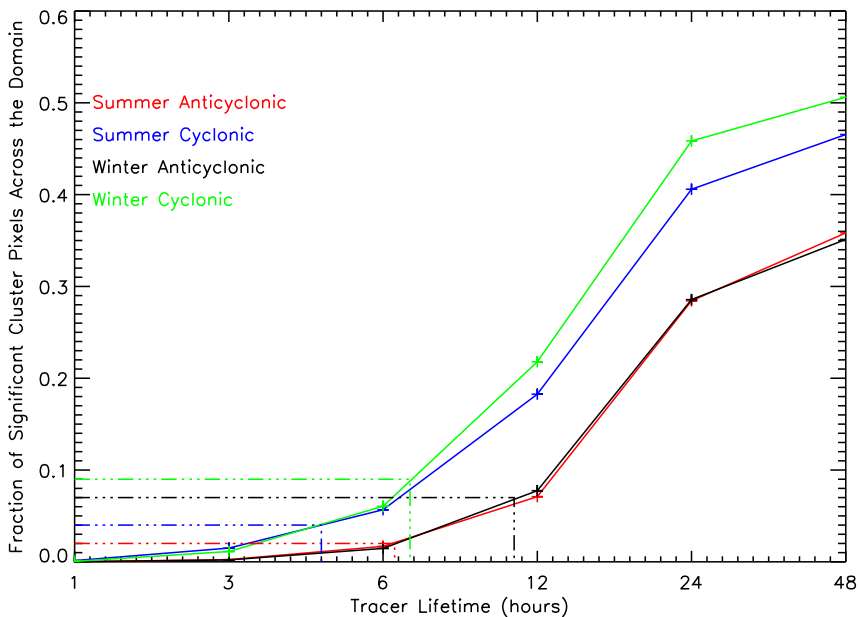
Figure 11. Proportion of the AQUM domain covered by significant anomaly pixels as a function of tracer lifetime for the different seasonal synoptic regimes. Red, blue, black and green represents the summer anticyclonic, summer cyclonic, winter anticyclonic and winter cyclonic conditions, respectively. Dashed lines represent the approximate life time of AQUM column NO_2 under the seasonal synoptic regimes based on the domain proportion of significant anomalies (pixels) in Figure 7.
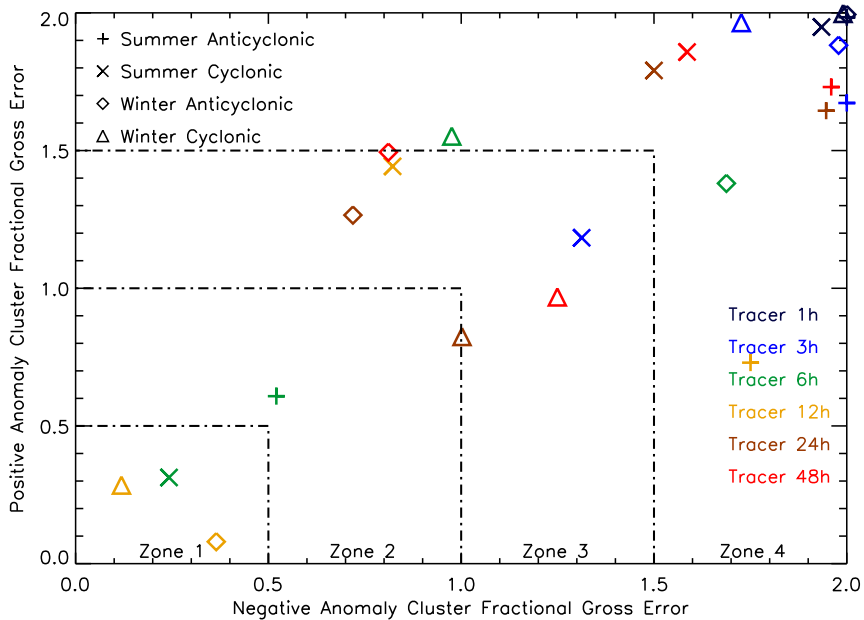
Figure 12. The same as Fig. 8, but for the anomaly cluster densities of AQUM column NO_2 – AQUM tracer columns. The different colours refer to the AQUM tracer experiments with e-folding lifetimes of 1, 3, 6, 12, 24 and 48 h.